PNAS RESEARCH ARTICLE | CELL BIOLOGY OPEN ACCESS

Ferroptosis regulation by the NGLY1/NFE2L1 pathway

Giovanni C. Forcina[a], Lauren Pope[a], Magdalena Murray[a], Wentao Dong[b,c], Monther Abu-Remaileh[b,c], Carolyn R. Bertozzi[c,d,e], and Scott J. Dixon[a,1]

Edited by Vishva Dixit, Genentech, San Francisco, CA; received October 12, 2021; accepted January 20, 2022

Ferroptosis is an oxidative form of nonapoptotic cell death whose transcriptional regulation is poorly understood. Cap'n'collar (CNC) transcription factors including nuclear factor erythroid-2–related factor 1 (NFE2L1/NRF1) and NFE2L2 (NRF2) are important regulators of oxidative stress responses. NFE2L1 abundance and function are regulated posttranslationally by N-glycosylation. Functional maturation of NFE2L1 requires deglycosylation by cytosolic peptide:N-glycanase 1 (NGLY1). We find that NGLY1 and NFE2L1 work in a common pathway to enhance ferroptosis resistance, independent of NFE2L2, by promoting expression of the key antiferroptotic enzyme glutathione peroxidase 4 (GPX4). Enhanced ferroptosis sensitivity in NFE2L1-knockout cells can be reverted by expression of an NFE2L1 mutant containing eight asparagine-to-aspartate protein sequence substitutions, which mimic NGLY1-catalyzed protein sequence editing. These results suggest that ferroptosis sensitivity may be regulated by NGLY1-catalyzed NFE2L1 deglycosylation. These results highlight a role for the disease-associated NGLY1/NFE2L1 pathway in ferroptosis regulation.

ferroptosis | NRF1 | cancer

Significance

Ferroptosis is an oxidative form of cell death whose biochemical regulation remains incompletely understood. Cap'n'collar (CNC) transcription factors including nuclear factor erythroid-2–related factor 1 (NFE2L1/NRF1) and NFE2L2/NRF2 can both regulate oxidative stress pathways but are each regulated in a distinct manner, and whether these two transcription factors can regulate ferroptosis independent of one another is unclear. We find that NFE2L1 can promote ferroptosis resistance, independent of NFE2L2, by maintaining the expression of glutathione peroxidase 4 (GPX4), a key protein that prevents lethal lipid peroxidation. NFE2L2 can also promote ferroptosis resistance but does so through a distinct mechanism that appears independent of GPX4 protein expression. These results suggest that NFE2L1 and NFE2L2 independently regulate ferroptosis.

Ferroptosis is an oxidative, nonapoptotic cell death pathway activated in several distinct acute and chronic pathophysiological cell death contexts (1). Ferroptosis can be triggered by depletion of cystine (the oxidized form of cysteine), which is necessary for the synthesis of the antiferroptotic metabolites glutathione (GSH) and coenzyme A, or by direct inactivation of the GSH-dependent lipid hydroperoxidase glutathione peroxidase 4 (GPX4) (2–4). Cystine depletion and/or GPX4 inactivation result in the iron-dependent accumulation of lipid peroxides at the plasma membrane and other sites within the cell, ultimately resulting in membrane permeabilization (2, 5, 6). The factors that modulate ferroptosis sensitivity by impinging on key regulators like GPX4 are incompletely understood. It is of great interest to identify factors that govern ferroptosis sensitivity, as these may suggest novel points of intervention to either enhance or inhibit this process therapeutically.

The cap'n'collar (CNC) family of transcription factors is highly conserved among metazoans and plays an important role in maintaining homeostasis in response to stress (7). Vertebrates express several CNC family transcription factors, including the related nuclear factor erythroid-2–related factor 1 NFE2L1 (NRF1) and NFE2L2 (NRF2) proteins. NFE2L2 is considered the master antioxidant transcription factor and can inhibit ferroptosis by regulating the expression of the cystine/glutamate antiporter subunit *SLC7A11*, glutamate–cysteine ligase (GCL) subunits *GCLC* and *GCLM*, and other effectors (8–15). Interestingly, however, *Nfe2l2* is not essential for development in mice, and adult animals exhibit only minor phenotypic abnormalities compared with disruption of *Nfe2l1*, which is embryonic lethal (16, 17). This suggests that NFE2L2 and NFE2L1 may harbor nonredundant roles, at least in some contexts (e.g., mouse development). NFE2L1 is canonically viewed as a regulator of proteasome-subunit gene expression, but like NFE2L2 can also regulate the expression of several antioxidant genes (18–22). Whether NFE2L1 can regulate ferroptosis sensitivity similar to NFE2L2 is not known.

NFE2L2 and NFE2L1 protein abundance are both regulated posttranslationally, but in distinct manners. NFE2L2 is regulated by its cytoplasmic inhibitor Kelch-like ECH-associating protein 1 (KEAP1) (23). KEAP1 binds and sequesters NFE2L2 in the cytosol and targets it for proteolytic degradation (24, 25). NFE2L1 is not regulated by KEAP1. Rather, NFE2L1 is constitutively translated into the endoplasmic reticulum (ER), N-glycosylated by oligosaccharyltransferase, translocated from the lumen of the ER into the cytosol, deglycosylated by N-glycanase 1 (NGLY1), released from the ER membrane into the cytosol by DNA damage inducible 1 homolog 2 (DDI2), and then mostly constitutively degraded by the proteasome (26, 27). Of note, the NGLY1-catalyzed deglycosylation reaction leads to "editing" of previously glycosylated Asn residues to Asp residues, a modification that is necessary for the *Caenorhabditis elegans*

Author contributions: G.C.F., M.A.-R., C.R.B., and S.J.D. designed research; G.C.F. and W.D. performed research; L.P., M.M., and C.R.B. contributed new reagents/analytic tools; G.C.F. and S.J.D. analyzed data; and G.C.F. and S.J.D. wrote the paper.

Competing interest statement: C.R.B. is a cofounder and scientific advisory board member of Palleon Pharmaceuticals, Enable Biosciences, Redwood Bioscience (a subsidiary of Catalent), and InterVenn Biosciences, and a member of the board of directors of Eli Lilly and Company. S.J.D. is a cofounder of Prothegen and a scientific advisory board member of Ferro Therapeutics and Hillstream Biopharma, and holds patents related to ferroptosis.

This article is a PNAS Direct Submission.

[1]To whom correspondence may be addressed. Email: sjdixon@stanford.edu.

This article contains supporting information online at http://www.pnas.org/lookup/suppl/doi:10.1073/pnas.2118646119/-/DCSupplemental.

Published March 10, 2022.

NFE2L1 ortholog SKN-1A to regulate proteasome gene expression (28). Biallelic *NGLY1* mutation causes an ultrarare human disorder called Ngly1 deficiency, characterized by intellectual disability, hyperkinetic movement disorder, liver dysfunction, and alacrima (29). NGLY1 disruption has been associated with defects in mitochondrial homeostasis and inflammatory responses (30, 31), 5′ adenosine monophosphate–activated protein kinase signaling (32), plasma membrane transporter function (33, 34), and BMP4 signaling (35). How altered NFE2L1 glycosylation and function may contribute to phenotypes observed in NGLY1-mutant models and patients, such as increased oxidative stress (36), are not well-understood.

Here, we report that the NGLY1/NFE2L1 pathway regulates ferroptosis sensitivity in human cancer cells, in parallel to NFE2L2. NGLY1 is necessary to promote NFE2L1 stability and inhibit ferroptosis. This process may involve protein sequence editing, as an Asn-to-Asp NFE2L1-mutant protein is sufficient to potently inhibit ferroptosis. Cells lacking NGLY1 or NFE2L1 are sensitized to ferroptosis due to loss of GPX4 protein expression. NFE2L1 expression is unable to inhibit ferroptosis in cells lacking GPX4. By contrast, NFE2L2 can partially inhibit ferroptosis in the absence of GPX4 expression. These results highlight potentially distinct roles for NFE2L1 and NFE2L2 in ferroptosis regulation. Our results also suggest that enhanced sensitivity to ferroptosis or other types of oxidative stress could be relevant to phenotypes observed in patients with NGLY1 mutations.

Results

Disruption of CNC Transcription Factors Sensitizes to Ferroptosis. NFE2L2 and NFE2L1 have nonredundant functions in mammalian development (16, 17). Whether the KEAP1/NFE2L2 and NGLY1/NFE2L1 pathways could operate independently to regulate ferroptosis was unclear. To establish a baseline for comparison, we first focused on the ability of the KEAP1/NFE2L2 pathway to modulate ferroptosis sensitivity. *KEAP1* mutation leads to NFE2L2 accumulation (24, 25). Using data available through the DepMap portal (37, 38), we observed a correlation across over 700 cancer cell lines between *KEAP1* mutation and resistance (i.e., higher median area under the curve [AUC] values) to two mechanistically distinct ferroptosis-inducing small molecules, the system x_c^- inhibitor erastin and the covalent GPX4 inhibitor ML162 (Fig. 1 *A* and *B*). This suggested that high NFE2L2 expression may globally correlate with ferroptosis resistance in cancer cells.

To investigate further, we examined human KEAP1-mutant A549 cells, which accumulate high levels of NFE2L2 constitutively (39). We isolated two clonal A549 cell lines where *NFE2L2* was disrupted (i.e., "knocked out"; KO) using CRISPR-Cas9 technology, as well as two clonal control cell lines that underwent the CRISPR process but expressed NFE2L2 normally (Fig. 1*C*). To amplify our ability to detect NFE2L2, we treated cells with the proteasome inhibitor bortezomib, which caused the expected accumulation of NFE2L2 in Control1/2 cells but not in $NFE2L2^{KO1/2}$ cells (40) (Fig. 1*C*). To examine cell death, we transduced all four cell lines with lentivirus directing the expression of the live-cell marker nuclear-localized mKate2 (denoted by the superscript "N") that, together with incubation with the dead-cell dye SYTOX Green, enabled cell death to be directly quantified over time using the scalable time-lapse analysis of cell death kinetics (STACK) method (*SI Appendix*, Fig. S1*A*) (41, 42). Compared with $Control1/2^N$ cell lines, $NFE2L2^{KO1/2,N}$ cell lines exhibited a >100-fold heightened sensitivity to the more potent erastin analog erastin2, and to ML162 (Fig. 1*D* and *SI Appendix*, Table S1; note: *SI Appendix*, Table S1 contains half-maximal effective concentration values for all dose–response curves in this work). Ferroptosis was also initiated more rapidly in $NFE2L2^{KO1/2,N}$ cells compared with $Control1/2^N$ cells, as determined using STACK analysis (*SI Appendix*, Fig. S1 *B* and *C*). We confirmed that cell death under these conditions was ferroptosis, as it was fully suppressed by the specific ferroptosis inhibitor ferrostatin-1 (Fer-1) (Fig. 1*D*). The enhanced ferroptosis sensitivity of $NFE2L2^{KO1,N}$ cells was reverted by expression of wild-type *NFE2L2* complementary DNA (cDNA), which also enhanced ferroptosis resistance when introduced into $Control1^N$ cells (Fig. 1 *E* and *F*). Disruption of NFE2L1 had no effect on the lethality of camptothecin, an apoptosis inducer (Fig. 1*F*). These results indicate that NFE2L2 is a potent negative regulator of ferroptosis in A549 cells.

We next turned to investigate the role of NFE2L1 in ferroptosis. For these studies, we continued to employ A549 cells as a model, as constitutive accumulation of high NFE2L2 protein levels would allow us to readily ascertain whether disruption of NFE2L1 resulted in any nonredundant phenotypes. Using CRISPR-Cas9 technology and single-cell sorting, we isolated two independent NFE2L1 gene-disrupted clones (Fig. 1*G*). We transduced these two cell lines, as well as two unmodified control cell lines, with mKate2 lentivirus to enable analysis of cell death using STACK. NFE2L1 is constitutively degraded by the proteasome and was barely detectable by Western blot in unmodified $Control1/2^N$ cells (Fig. 1*G*). Treatment with bortezomib resulted in the expected accumulation of NFE2L1 protein in $Control1/2^N$ cells but not $NFE2L1^{KO1/2,N}$ cell lines (Fig. 1*G*) (26). Strikingly, $NFE2L1^{KO1/2,N}$ cell lines were much more sensitive to erastin2 and ML162 compared with $Control1/2^N$ cell lines, with these compounds causing an earlier onset of cell death across a range of lethal concentrations (Fig. 1*H* and *SI Appendix*, Fig. S1 *D* and *E*). This ferroptosis sensitivity phenotype was reverted in $NFE2L1^{KO1,N}$ cells by lentivirus-mediated stable reexpression of wild-type NFE2L1 (Fig. 1 *I* and *J*). Notably, NFE2L1 overexpression in $Control1^N$ cells increased NFE2L1 levels and enhanced ferroptosis resistance (Fig. 1 *I* and *J*). NFE2L1 expression appeared to have a relatively specific effect on ferroptosis sensitivity, as disruption of this gene significantly sensitized to erastin, erastin2, ML162, and a distinct GPX4 inhibitor, RSL3, but few other compounds from a library of 261 bioactive molecules (Fig. 1*K*). We conclude that NFE2L1 can inhibit ferroptosis in a specific manner independent of NFE2L2.

Proteasome inhibition causes NFE2L1 accumulation, which then can induce a bounce-back response involving the increased expression of various proteasomal genes (21, 22, 26). NFE2L1 can also regulate the expression of various antioxidant genes (19, 20). We wondered whether proferroptotic oxidative stress itself could trigger NFE2L1 accumulation, and whether this influenced ferroptosis sensitivity. Unlike bortezomib, neither erastin2 nor ML162 triggered NFE2L1 accumulation alone, and combinations of these agents with bortezomib did not further increase NFE2L1 protein levels (Fig. 1*L*). Thus, basal NFE2L1 protein that escapes proteasomal degradation appeared sufficient to inhibit ferroptosis, with greater accumulation of this transcription factor not conferring any additional protection.

Protein Sequence–Edited NFE2L1 Promotes Ferroptosis Resistance. NFE2L1 is subject to complex posttranslational regulation, including N-glycosylation and subsequent deglycosylation by NGLY1 (26) (Fig. 2*A*). NGLY1-mediated deglycosylation is of special interest, as mutation of this enzyme causes an ultrarare developmental disorder whose etiology is not well-understood.

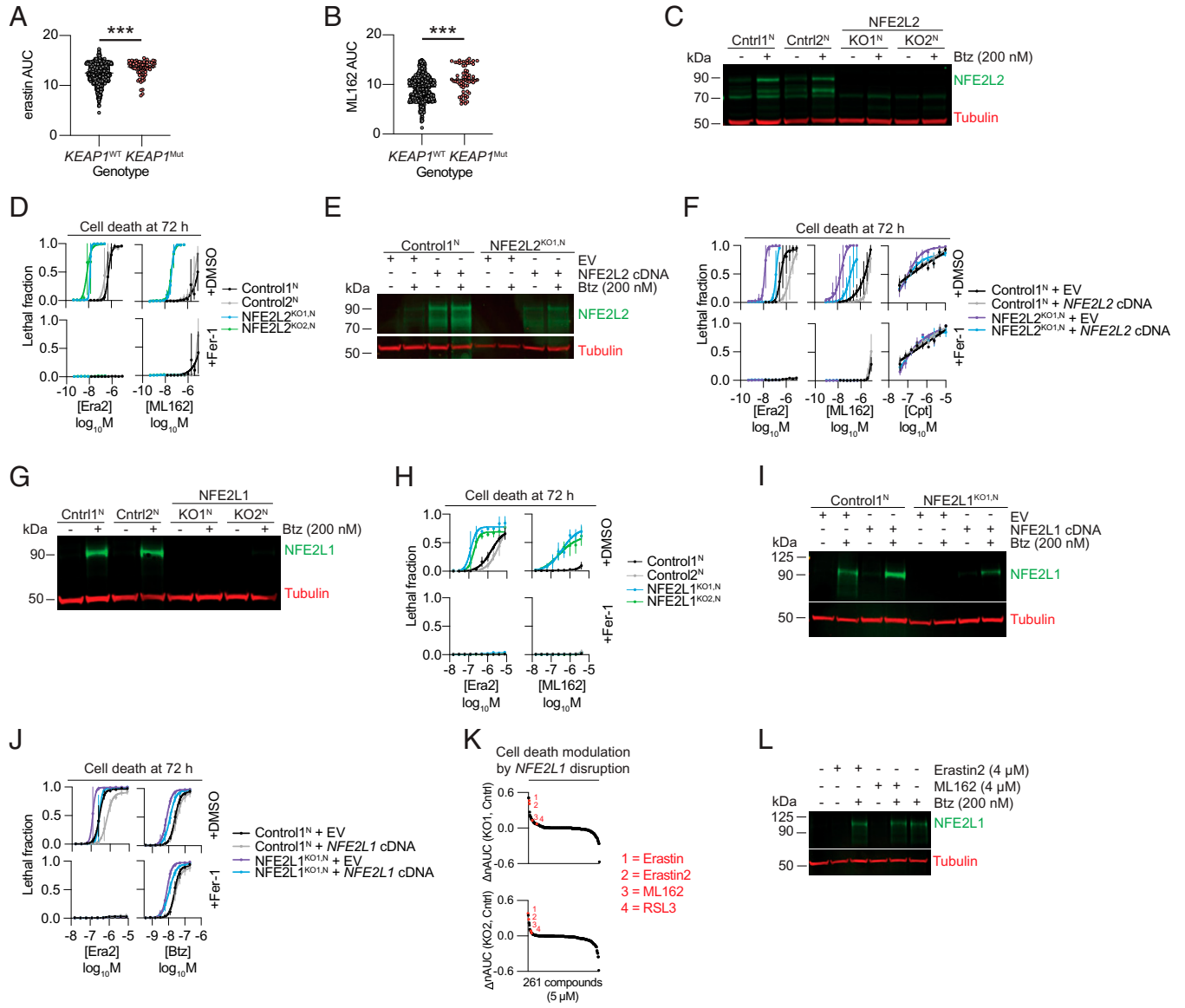

Fig. 1. NFE2L2 and NFE2L1 negatively regulate ferroptosis. (*A* and *B*) Correlation between *KEAP1* mutation status and sensitivity to ferroptosis inducers erastin or ML162. Data are derived from the DepMap portal. Each data point represents a single cell line. Higher AUC values indicate lower sensitivity to compound treatment. WT, wild type. Mut, mutant. (*C*) Protein levels in A549 Control^{N} and NFE2L2$^{KO1/2,N}$ cell lines treated ± the proteasome inhibitor bortezomib (Btz). (*D*) Cell death in A549 Control^{N} and NFE2L2$^{KO1/2,N}$ cell lines. Era2, erastin2. (*E*) Protein levels in A549 Control1^{N} and NFE2L2^{KO1,N} cells stably transduced with empty vector (EV) lentivirus or lentivirus directing the expression of NFE2L2. (*F*) Cell death in A549 Control1^{N} and NFE2L2^{KO1,N} cells described in *E*. Cpt, camptothecin. (*G*) Protein levels in A549 Control1/2^{N} and NFE2L1$^{KO1/2,N}$ cell lines treated as indicated. (*H*) Cell death in A549 Control1/2^{N} and NFE2L1$^{KO1/2,N}$ cell lines. (*I*) Protein levels in A549 Control1^{N} and NFE2L1^{KO1,N} cells transduced with EV lentivirus or lentivirus directing the expression of NFE2L1. (*J*) Cell death in A549 Control1^{N} and NFE2L1^{KO1,N} cells described in *I*. (*K*) Difference (delta) in normalized area under the curve (nAUC) lethal fraction values for A549 NFE2L1$^{KO1/2,N}$ versus Control1^{N} cells after treatment with 261 different bioactive small molecules (5 μM). Higher ΔnAUC values indicate greater death sensitivity in NFE2L1$^{KO1/2,N}$ versus Control1^{N} cell lines. (*L*) Effect of ferroptosis inducers on NFE2L1 protein levels. A549 cells were treated with vehicle (DMSO), erastin2 (4 μM), or ML162 (4 μM) ± Btz (200 nM) for 4 h. (*C*, *E*, *G*, and *I*) Treatment was ±Btz for 4 h. (*D*, *L*, *H*, and *J*) Fer-1 was used at 1 μM. Data represent mean ± SD of three (*D* and *H*) or four (*F* and *J*) independent experiments. Data in *K* represent the average ΔnAUC of three biological replicates. ***$P \leq 0.001$.

Whether NGLY1 disruption would impact ferroptosis sensitivity was unclear. To investigate, we generated clonal *NGLY1* gene-disrupted cell lines that also expressed nuclear-localized mKate2 (i.e., NGLY1$^{LOF1/2,N}$). We observed no detectable NGLY1 protein, reduced NFE2L1 protein abundance, and a higher molecular-mass NFE2L1 protein species corresponding to its glycosylated form in both NGLY1$^{LOF1/2}$ cell lines (Fig. 2*B*). DNA sequencing of the *NGLY1* genomic locus to confirm mutation was unsuccessful. We therefore refer to these clones as "loss-of-function" (LOF) rather than KO. Indeed, there remained some deglycosylated NFE2L1 in the NGLY1$^{LOF1/2}$ cells (Fig. 2*B*). This suggested that these cell lines may be NGLY1 hypomorphs rather than true protein nulls. Nevertheless, both NGLY1$^{LOF1/2,N}$ cells showed enhanced sensitivity to erastin2-induced ferroptosis (Fig. 2*C*). Loss of NGLY1 also enhanced ferroptosis sensitivity in HEK293 cells and mouse embryonic fibroblasts, while having no effect in HepG2 cells (*SI Appendix*, Fig. S2).

NGLY1 and NFE2L1 operate within the same pathway to modulate sensitivity to bortezomib-induced cell death (26). We hypothesized that NGLY1 and NFE2L1 would likewise operate in the same pathway to suppress ferroptosis. To test this hypothesis, we generated Control1^{N} and NFE2L1^{KO1,N} cell lines transduced with lentivirus directing the overexpression of NGLY1 (Fig. 2*D*). Control1^{N} cells overexpressing NGLY1 were more resistant to erastin2-induced ferroptosis than Control1^{N} cells transduced with an empty vector (EV) control (Fig. 2*E*). Consistent with

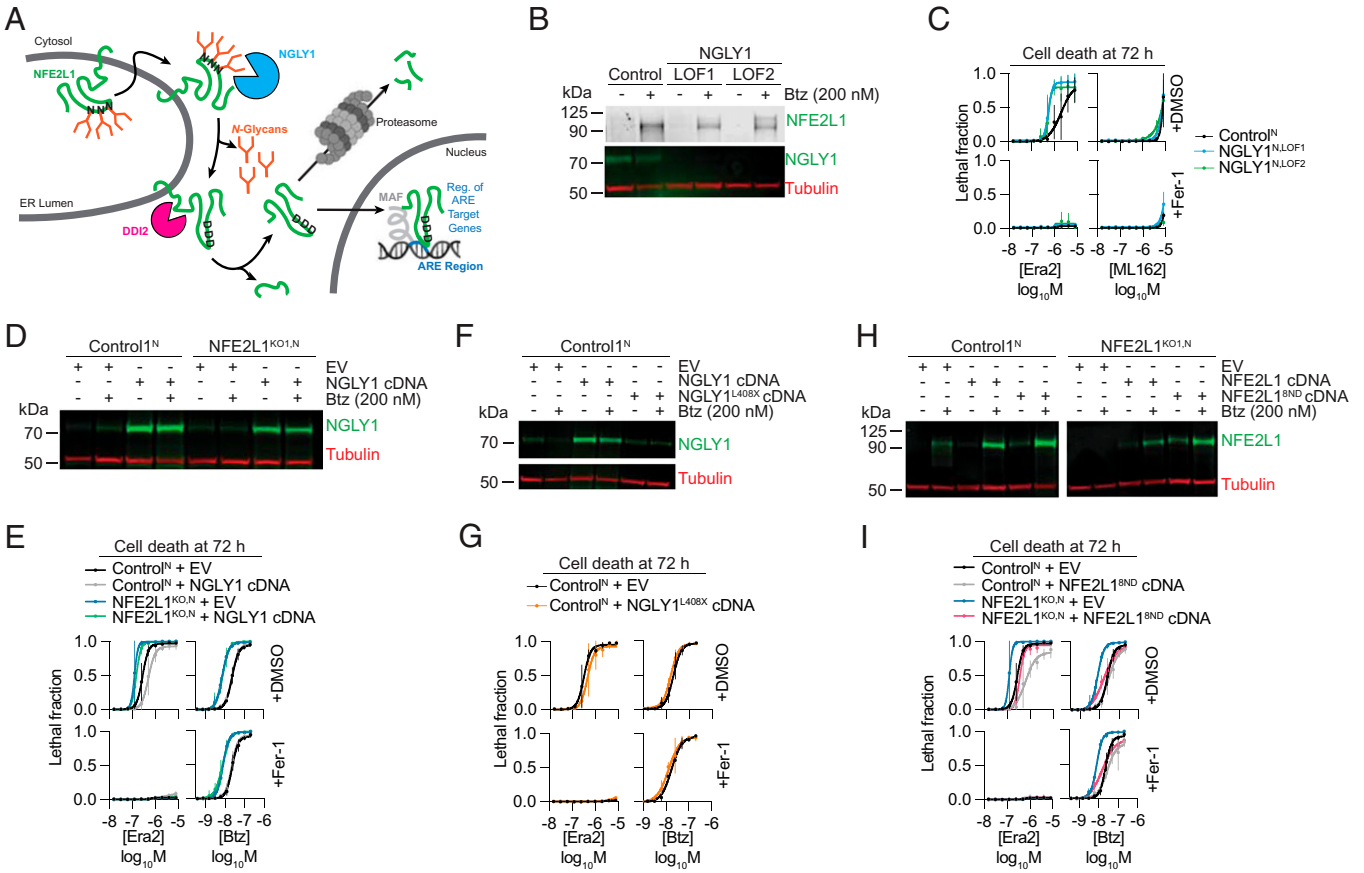

Fig. 2. NGLY1-mediated protein sequence editing of NFE2L1 regulates ferroptosis. (*A*) Schematic of NFE2L1 processing and activation, adapted from ref. 26. MAF, bZIP transcription factors that heterodimerize with NFE2L1. ARE, antioxidant response element. (*B*) Protein levels in A549 Control^{N} and NGLY1$^{KO1/2,N}$ cell lines. (*C*) Cell death in A549 Control^{N} and NGLY1$^{KO1/2,N}$ cell lines. (*D*) Protein levels in A549 Control1^{N} and NFE2L1^{KO1,N} cells stably transduced with EV lentivirus control or lentivirus directing the expression of NGLY1. (*E*) Cell death in cell lines described in *D*. (*F*) Protein levels in A549 Control1^{N} cells stably transduced with EV lentivirus control or lentivirus directing the expression of wild-type NGLY1 or NGLY1^{L408X}. (*G*) Cell death in cell lines described in *F*. (*H*) Protein levels in A549 Control1^{N} or NFE2L1^{KO1,N} cells stably transduced with EV lentivirus control, or lentivirus directing the expression of wild-type NFE2L1 or the sequence-edited NFE2L1^{8ND} mutant. (*I*) Cell death in cell lines described in *H*. (*B*, *D*, *F*, and *H*) Treatment was ±Btz for 4 h. (*C*, *G*, *E*, and *I*) Fer-1 was used at 1 μM. Data represent mean ± SD from three (*C*) or four (*E* and *I*) independent experiments.

NGLY1 operating upstream of NFE2L1, sensitivity to erastin2 in NFE2L1^{KO1,N} cells was unchanged by NGLY1 overexpression (Fig. 2*E*). Interestingly, unlike erastin2-induced ferroptosis, NGLY1 overexpression had no effect on bortezomib-induced cell death in Control1^{N} cells (Fig. 2*E*), suggesting that sensitivity to this lethal stimulus may not be regulated by the small pool of NFE2L1 that escapes proteasomal degradation. Unlike wild-type NGLY1, an NGLY1^{L408X} mutant, which results in a premature stop codon, was not expressed over background levels and did not inhibit ferroptosis in Control1^{N} cells (Fig. 2 *F* and *G*). These data are consistent with NGLY1 operating upstream of NFE2L1 to regulate sensitivity to ferroptosis.

In *C. elegans*, NGLY1/PNG-1–mediated deglycosylation of NFE2L1/SKN-1A results in a protein sequence–editing event where asparagine residues are converted to aspartic acid residues (28). This Asn-to-Asp editing is required for NFE2L1/SKN-1A to protect against bortezomib-induced cell death (28). In *C. elegans*, SKN-1A has four potential N-glycosylation sites. The human NFE2L1 protein is considerably larger and contains at least eight potential sites of N-glycosylation (predicted by conserved N-glycosylation motifs NxS/T, where x is any amino acid except proline). Which, if any, of these sites were important for NFE2L1 ferroptosis regulation was unclear. To investigate, we stably expressed an edited NFE2L1 construct where eight predicted glycosylated Asn residues were converted to Asp (NFE2L1^{8ND}), mimicking NGLY1-dependent processing. We expressed wild-type NFE2L1 and NFE2L1^{8ND} in both Control1^{N} and NFE2L1^{KO1,N} cells via lentiviral transduction. NFE2L1^{8ND} appeared more stable than wild-type NFE2L1, as we were able to detect significant levels of the mutant protein by Western blot in the absence of proteasome inhibition (Fig. 2*H*). We infer that the presence of N-glycans on NFE2L1 may promote its degradation, in accord with recent data acquired for a mutant NFE2L1 protein with nine Asn-to-Asp mutations (43). With respect to ferroptosis, both Control1^{N} and NFE2L1^{KO1,N} cells expressing NFE2L1^{8ND} displayed enhanced resistance to cell death induced by bortezomib or erastin2 (Fig. 2*I*). These results indicate that an NFE2L1 deglycosylation mimic is sufficient to inhibit cell death.

The NGLY1/NFE2L1 Pathway Regulates GPX4 Protein Levels. We next sought to determine how NFE2L1 regulated ferroptosis sensitivity. We initially hypothesized that NFE2L1 would directly regulate the expression of some key ferroptosis-related gene. Thus, we used RNA sequencing (RNA-seq) to analyze gene expression in A549 Control1^{N} and NFE2L1$^{KO1/2,N}$ cells. As a control, we found that expression of numerous proteasome-subunit genes was altered in response to bortezomib treatment in Control1 but not NFE2L1$^{KO1/2}$ cells, consistent with expectations (22) (*SI Appendix*, Fig. S3). Since our earlier results suggested that basal NFE2L1 expression was sufficient to regulate ferroptosis sensitivity (Fig. 1 *G* and *H*), we focused on basal differences in gene expression between Control1 and NFE2L1$^{KO1/2}$ cells. In total, the

expression of 97 genes was significantly altered ($P_{adj} < 0.05$) in both NFE2L1$^{KO1/2}$ KO lines compared with the Control1 cell line, with 56 genes increased and 41 genes decreased (Gene Expression Omnibus [GEO] accession no. GSE182461). However, disruption of NFE2L1 did not significantly decrease the expression of the cystine/glutamate antiporter *SLC7A11*, ferroptosis suppressor protein 1 (*FSP1/AIFM2*), or several GSH biosynthetic genes (*GCLC*, *GCLM*, *GSS*), suggesting that altered expression of antiferroptotic genes might not explain the observed ferroptosis sensitization phenotype in the absence of NFE2L1.

Given these results, we considered the possibility that NFE2L1 modulated ferroptosis in an indirect manner, by altering the expression of key ferroptosis-related proteins. To investigate, we examined the levels of various proteins by Western blotting. Here, we also compared the effects of NFE2L1 disruption with NFE2L2 disruption to see whether these two transcription factors had similar or unique effects on the expression of key proteins. For this analysis, we included canonical NFE2L2 target gene products (e.g., HMOX1), key ferroptosis-associated gene products, some of which are known NFE2L2 targets (e.g., GCLC, GCLM), and GPX4 (Fig. 3*A*; quantification for all proteins and conditions is in *SI Appendix*, Fig. S4*A*). Disruption of NFE2L1 but not NFE2L2 resulted in decreased HO-1 expression, consistent with the possibility of redundant transcription factor effects. Indeed, loss of NFE2L1 had little quantitative effect on the expression of GCLM or GCLC, while disruption of NFE2L2 resulted in strong loss of GCLC expression, consistent with previous analyses of mouse embryonic fibroblasts (20), but little change in GCLM expression in these cells. Strikingly, we observed a marked decrease in GPX4 protein expression in NFE2L1$^{KO1/2}$ cell lines versus both the control cell line and NFE2L2 gene-disrupted cell lines. Bortezomib treatment, included as a positive control for NFE2L1 accumulation, did not consistently alter the expression of HO-1, GCLM, GCLC, or GPX4 in any cell line (Fig. 3*C* and *SI Appendix*, Fig. S4*A*). These results indicated that NFE2L1 and NFE2L2 can differentially regulate the levels of key ferroptosis-related proteins, most notably GPX4 (in the case of NFE2L1) and GCLC (in the case of NFE2L2).

Based on our results, we sought to understand how NFE2L1 and NFE2L2 could each regulate ferroptosis sensitivity. We first focused on NFE2L2. Above, we observed that disruption of NFE2L2 lowered expression of GCLC, the catalytic subunit of the rate-limiting GSH biosynthetic enzyme GCL (44). Accordingly, we hypothesized that NFE2L2 disruption sensitized to ferroptosis by reducing GSH abundance. Consistent with this hypothesis, loss of NFE2L2 greatly reduced intracellular GSH, almost to the levels obtained following treatment of control cells with erastin2, while disruption of NFE2L1 had no such effect (Fig. 3*B*). Pretreatment with the GCL inhibitor buthionine sulfoximine (BSO) potently sensitized both NFE2L2^{KO1,N} and NFE2L1^{KO1,N} cells to erastin2-induced ferroptosis, with a slightly stronger effect observed in the former versus the latter cell line (Fig. 3*C*). This is consistent with GSH being an important negative regulator of ferroptosis whose basal depletion renders NFE2L2-mutant cells hypersensitive to further loss of this metabolite.

As GSH levels were not strongly reduced in cells lacking NFE2L1, this left unanswered how these cells were sensitized to ferroptosis. Notably, we observed a striking decrease in GPX4 protein levels in NFE2L1$^{KO1/2}$ cells compared with Control1/2 cells and NFE2L2 gene-disrupted cell lines (Fig. 3*A* and *SI Appendix*, Fig. S4*A*). GPX4 levels were also reduced in NGLY1$^{LOF1/2,N}$ lines compared with Control^{N} cells (Fig. 3*D*; see quantification in *SI Appendix*, Fig. S4*B*). Accordingly, we hypothesized that loss of GPX4 protein upon NGLY1/NFE2L1 pathway disruption sensitized cells to ferroptosis. To test this hypothesis, we generated Control1^{N} and NFE2L1^{KO1,N} lines stably overexpressing the cytosolic isoform of GPX4 (cGPX4), which was previously shown to inhibit ferroptosis when overexpressed in other contexts (2). We observed that cGPX4 overexpression reverted the enhanced ferroptosis sensitivity of NFE2L1^{KO1,N} cells, with no effect on bortezomib toxicity (Fig. 3 *E* and *F*). We probed GPX4 protein levels in Control1 cells and NFE2L1^{KO1} cells stably transduced with EV control or lentivirus directing the expression of wild-type NFE2L1 or NFE2L1^{8ND}. Remarkably, expression of NFE2L1 and NFE2L1^{8ND} could restore GPX4 protein expression to levels like those observed in Control1^{N} cells (Fig. 3*G*; see quantification in *SI Appendix*, Fig. S4*C*). Of note, this effect appeared to be indirect, as expression of NFE2L1 and NFE2L1^{8ND} had little ability to increase *GPX4* messenger RNA expression relative to vector control cells (*SI Appendix*, Fig. S4*D*).

NFE2L1 can regulate the expression of numerous antioxidant genes, any one of which could be necessary to suppress ferroptosis (20). To test whether GPX4 alone was necessary for suppression of ferroptosis, we stably transduced HT-1080 fibrosarcoma Control^{N} and GPX4^{KO,N} cells with lentivirus directing the expression of wild-type NFE2L1, NFE2L1^{8ND}, or, for comparison, wild-type NFE2L2 (Fig. 3 *H* and *I*). Similar to results obtained in A549 cells (Fig. 1*J*), HT-1080 Control^{N} cells overexpressing NFE2L1 or NFE2L1^{8ND} were less sensitive to the lethal effects of erastin2, ML162, or bortezomib (Fig. 3*J*). We then examined HT-1080 GPX4^{KO} cells, which must be cultured continually in medium containing Fer-1 to prevent cell death. In GPX4^{KO,N} cells cultured without Fer-1, overexpression of NFE2L1 or NFE2L1^{8ND} did not significantly inhibit ferroptosis (Fig. 3*K*). By contrast, NFE2L2 overexpression was able to partially suppress ferroptosis under these conditions (Fig. 3*K*), although it should be noted that we could obtain higher overexpression of this protein than of NFE2L1 (Fig. 3 *H* and *I*). Collectively, these results indicate that GPX4 is likely necessary and sufficient for the NGLY1/NFE2L1 pathway to inhibit ferroptosis, while NFE2L2 can inhibit ferroptosis in a manner that is partially independent of GPX4.

NFE2L2 Can Compensate for Disruption of the NGLY1/NFE2L1 Pathway. Our results suggested that NFE2L1 and NFE2L2 may regulate ferroptosis through distinct molecular mechanisms, and that NFE2L1 may regulate ferroptosis indirectly through effects on GPX4 protein levels. A related possibility was that disruption of NFE2L1 altered expression of NFE2L2. However, we observed little change in NFE2L1 protein levels in A549 NFE2L2^{KO} cells, and only a slight decrease in NFE2L2 levels in A549 NFE2L1^{KO} cells (Fig. 4*A*). Of note, bortezomib increased NFE2L2 levels in both A549 control and NFE2L1^{KO} cell lines, suggesting that this effect did not require NFE2L1 (Fig. 4*A*). These results suggested that loss of NFE2L1 did not sensitize to ferroptosis by disrupting basal NFE2L2 protein expression. However, these results led us to pose the question of whether high level NFE2L2 overexpression could be sufficient to functionally compensate for loss of NGLY1/NFE2L1 pathway activity. Accordingly, we generated A549 Control1^{N} and NFE2L1^{KO1,N} cells that stably overexpressed NFE2L2 and observed that this was sufficient to inhibit cell death triggered by erastin2 or ML162 but not bortezomib (Fig. 4 *B* and *C*). NFE2L2 overexpression was also sufficient to inhibit ferroptosis in A549 NGLY1^{LOF2,N} cells (Fig. 4 *D* and *E*), demonstrating a broad ability to functionally compensate for loss of NGLY1/NFE2L1 pathway activity. Finally, we investigated the opposite hypothesis, that NFE2L1 could reciprocally compensate

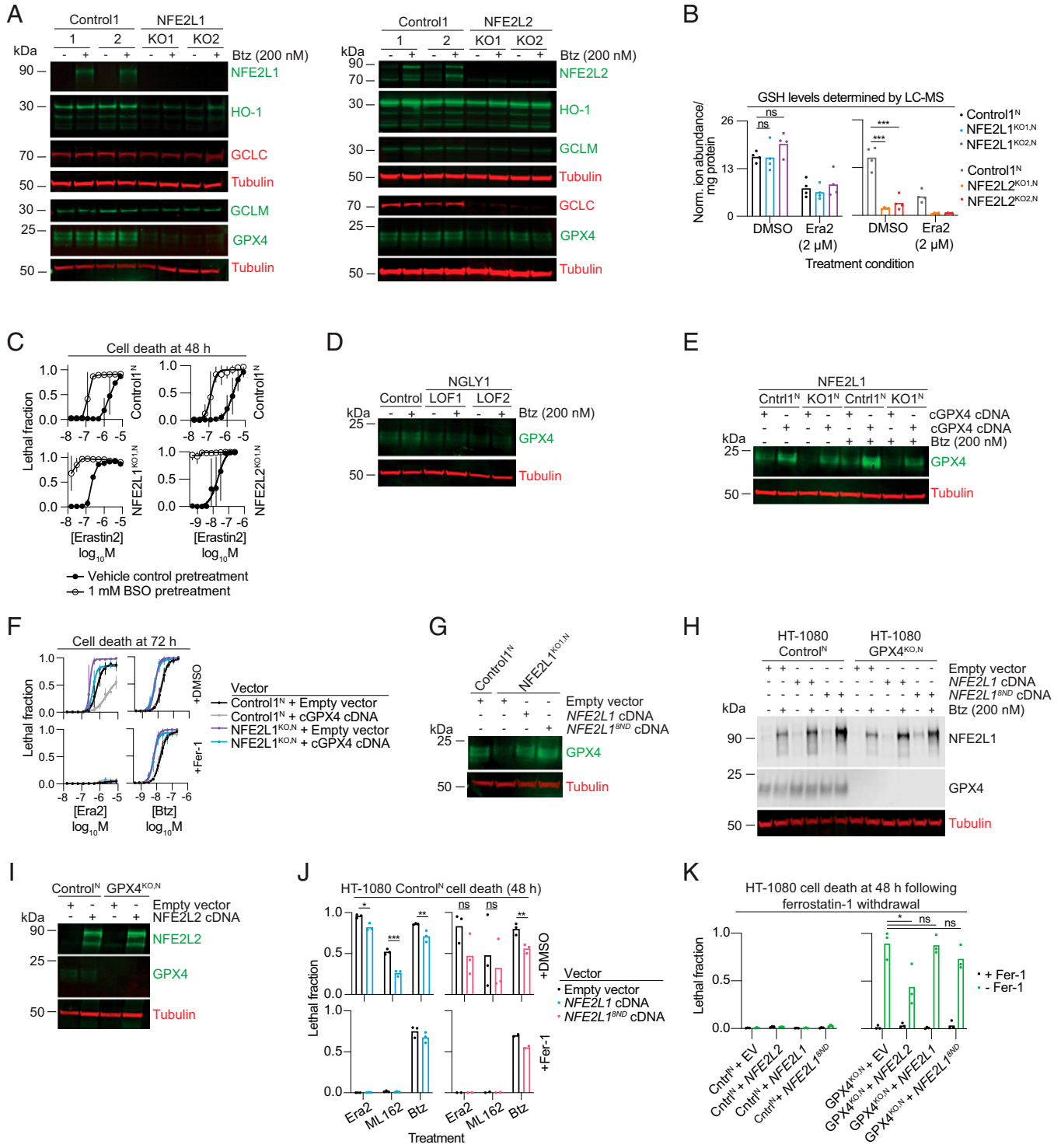

Fig. 3. NFE2L1 regulates ferroptosis via GPX4. (*A*) A549 cell protein expression in the indicated conditions. Note: The NFE2L2 panel (*A*, *Right*) is the same as shown in Fig. 1*C*, as other results were obtained from the same lysates. (*B*) Reduced GSH levels determined by liquid chromatography coupled to mass spectrometry (LC-MS) in A549 cell lines treated with vehicle (DMSO) or erastin2 (4 μM) for 4 h. (*C*) Cell death in A549 cell lines examined ± 24-h BSO pretreatment and the indicated conditions. (*D*) Protein expression in Control1^{N} and NGLY1$^{KO1/2,N}$ cells. (*E*) Protein expression in Control1^{N} (Cntrl1^{N}) and NFE2L1^{KO1,N} cells stably transduced with EV lentivirus control or lentivirus directing the expression of cGPX4. (*F*) Cell death in cell lines described in *E*. (*G*) Protein levels in A549 Control1^{N} and NFE2L1^{KO1,N} cell lines stably transduced with EV lentivirus control or lentivirus directing the expression of NFE2L1 or NFE2L1^{8ND}. (*H*) Protein levels in HT-1080 Control^{N} and GPX4^{KO,N} cell lines stably transduced with EV lentivirus control or lentivirus directing the expression of NFE2L1 or NFE2L1^{8ND}. (*I*) Protein levels in HT-1080 Control^{N} and GPX4^{KO,N} cell lines stably transduced with control EV lentivirus or lentivirus directing the expression of NFE2L2. (*J*) Cell death in stably transduced HT-1080 Control^{N} cells (from *I*) treated with erastin2 (125 nM), ML162 (250 nM), or bortezomib (100 nM). (*K*) Effect of NFE2L1 or NFE2L2 overexpression, as in *H* and *I*, respectively, on cell death in HT-1080 Control^{N} and GPX4^{KO,N} cells upon Fer-1 withdrawal. (*A*, *D*, *E*, and *H*) Treatment was ±Btz for 4 h. (*F*, *J*, and *K*) Fer-1 was used at 1 μM. *B*, *J*, and *K* depict individual data points from independent experiments. Data represent mean ± SD of two (*C*) or three (*F*) independent experiments. *$P \leq 0.05$, **$P \leq 0.01$, ***$P \leq 0.001$; ns, not significant.

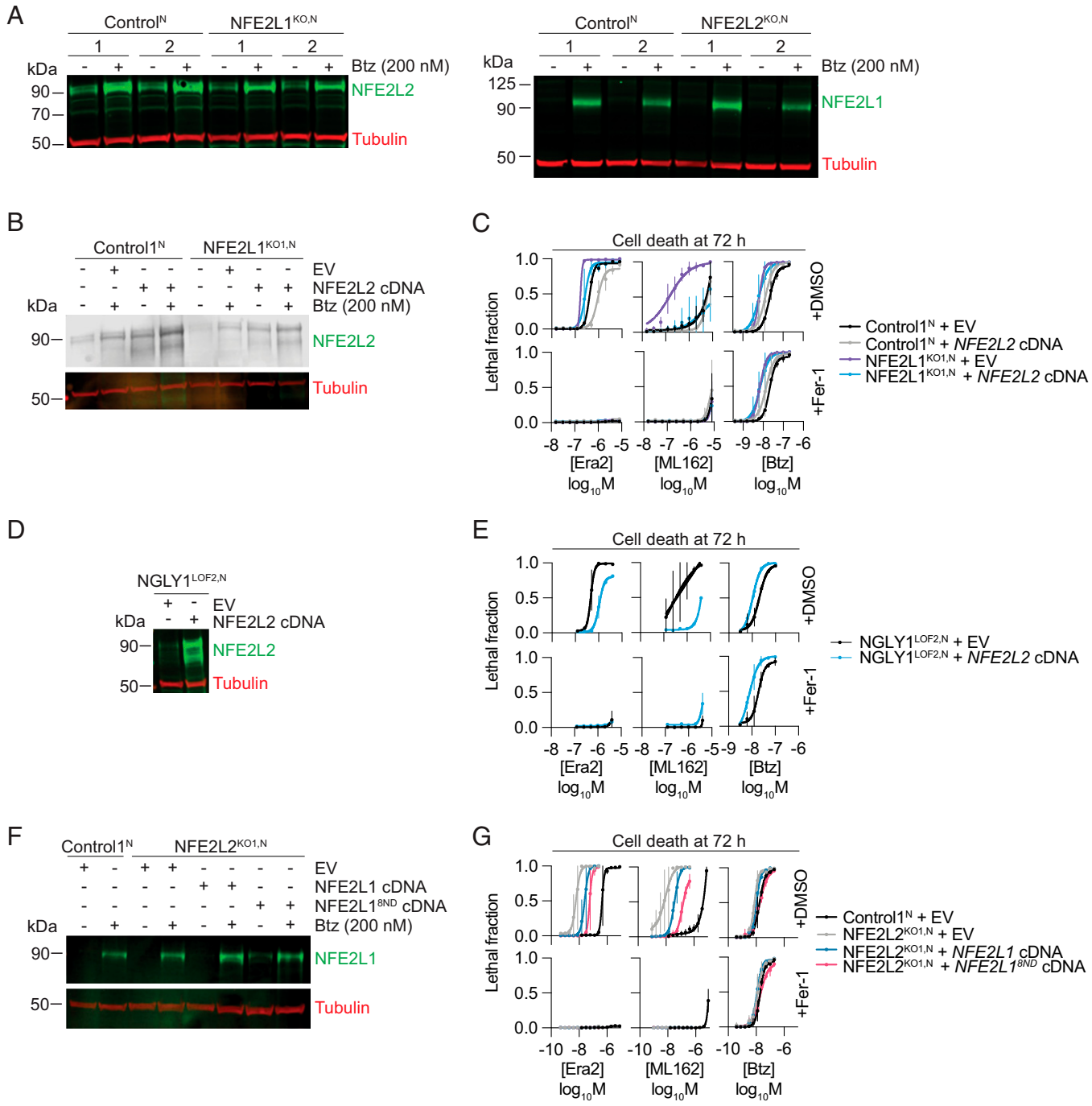

Fig. 4. Functional compensation between NFE2L1 and NFE2L2. (*A*, *Left*) Protein levels in A549 Control1/2^{N} and NFE2L1$^{KO1/2,N}$ cells. (*A*, *Right*) Protein levels in A549 Control1/2^{N} and NFE2L2$^{KO1/2,N}$ cells. (*B*) Protein levels in A549 Control1^{N} and NFE2L1^{KO1,N} cells stably transduced with EV lentivirus control or lentivirus directing the expression of NFE2L2. (*C*) Cell death in A549 Control1^{N} and NFE2L1^{KO1,N} cell lines described in *B*. (*D*) Protein levels in A549 Control1^{N} and NGLY1^{LOF2,N} cells stably transduced with EV lentivirus control or lentivirus directing the expression of NFE2L2. (*E*) Cell death in A549 Control1^{N} and NGLY1^{LOF1,N} cell lines described in *D*. (*F*) Protein levels in A549 Control1^{N} and NFE2L2^{KO1,N} cells stably transduced with EV lentivirus control or lentivirus directing the expression of wild-type NFE2L1 or mutant NFE2L1^{8ND}. (*G*) Cell death in A549 Control1^{N} and NFE2L2^{KO1,N} cell lines described in *F*. (*A*, *B*, and *F*) Treatment was ±Btz for 4 h. (*C*, *E*, and *G*) Fer-1 was used at 1 μM. Data represent mean ± SD of three (*C* and *G*) or two (*E*) independent experiments.

for loss of NFE2L2 in the regulation of ferroptosis sensitivity. We observed that expression of wild-type NFE2L1 or NFE2L1^{8ND} in A549 NFE2L2^{KO1,N} cells could partially revert the ferroptosis sensitization phenotype, with NFE2L1^{8ND} exhibiting the strongest effect (Fig. 4 *F* and *G*). Thus, in principle, NFE2L2 expression can compensate for disruption of the NGLY1/NFE2L1 pathway, and NFE2L1 can compensate for loss of NFE2L2 function in the prevention of ferroptosis, although specific mechanisms remain to be elucidated.

Discussion

Ferroptosis sensitivity is governed by several transcription factors, including p53 (45–47), YAP1/TAZ (48, 49), and NFE2L2 (8–11). In this work, we provide several lines of evidence that the NGLY1/NFE2L1 pathway can also antagonize ferroptosis, in parallel to the related KEAP1/NFE2L2 pathway. First, disruption of NGLY1 or NFE2L1 can sensitize to ferroptosis, even in cells that express high basal levels of NFE2L2

protein. Second, overexpression of wild-type NGLY1 can inhibit ferroptosis, but only when NFE2L1 is present. Third, the protein sequence–edited mimic of NFE2L1, NFE2L1^{8ND}, is sufficient to inhibit ferroptosis. These findings are consistent with NFE2L1 protein sequence editing being crucial for the function of this transcription factor (28, 43). It was recently suggested that a ninth Asn site (Asn574) of mammalian NFE2L1 is also edited by NGLY1, and that this is essential for the function of this transcription factor in the proteasome bounce-back response (43). We find that modification of the eight sites assayed here is sufficient to inhibit ferroptosis. It will be interesting in future studies to elucidate whether site-specific modifications, or cellular context, dictate unique biological outcomes associated with NFE2L1 glycosylation.

Our results suggest that the NGLY1/NFE2L1 pathway inhibits ferroptosis by promoting the expression of GPX4: Disruption of *NGLY1* or *NFE2L1* reduces GPX4 protein expression, and overexpression of GPX4 is sufficient to rescue ferroptosis sensitivity in *NFE2L1* mutants. This mechanism of ferroptosis regulation also appears distinct from how NFE2L2 functions, which in our models appears more tightly linked to the regulation of GSH synthesis through effects on the expression of *GCLC*. A notable observation is that the small amount of NFE2L1 that escapes constitutive proteasome-mediated degradation appears necessary and sufficient to inhibit ferroptosis. By contrast, engagement of the proteasome bounce-back response may require proteasome inhibition, leading to high levels of NFE2L1 accumulation (22, 26). A possibility consistent with our results is that the small basal NFE2L1 pool is more important for regulating oxidative stress, while a larger accumulation of NFE2L1 upon proteasome inhibition is needed to regulate proteasome gene expression.

NFE2L1 and NFE2L2 are structurally and functionally related. Indeed, we observe that NFE2L2 overexpression can complement the loss of NFE2L1, and NFE2L1 overexpression can partially complement for the loss of NFE2L2, with respect to ferroptosis sensitivity. The ability of NFE2L2 overexpression to partially rescue from ferroptosis in cells lacking GPX4 indicates that NFE2L2 can inhibit ferroptosis through non–GSH/GPX4-dependent mechanisms, which remain to be defined. Why endogenous NFE2L2 expression cannot fully complement the loss of NGLY1/NFE2L1 pathway activity remains unclear. One possibility which requires further investigation is that even KEAP1 mutation is not sufficient to elevate NFE2L2 protein accumulation to sufficiently high levels. Regardless, our results tentatively support the notion that compounds which cause the accumulation of NFE2L2 could provide a therapeutic benefit under conditions of NGLY1/NFE2L1 pathway dysfunction, as in Ngly1 deficiency (50). Indeed, it is possible that some of the beneficial effects of NFE2L2 activation observed in worm and fly models of Ngly1 deficiency (50) may be due to inhibition of ferroptosis or other forms of oxidative stress (36).

Materials and Methods

Chemicals and Reagents. A 261-member bioactive compound library was obtained from Selleck Chemicals (L2000), formatted as described previously (6), and stored at −80 °C. Erastin2 and ML162 were synthesized by Acme Bioscience. Chemicals used were dimethyl sulfoxide (DMSO) and Fer-1 (Sigma-Aldrich); Q-VD-OPh, bortezomib, and BSO (Thermo Fisher Scientific); and camptothecin and 1*S*,3*R*-RSL3 (RSL3) (Selleck Chemicals). BSO was dissolved directly into cell media. All other drugs were prepared as stock solutions in DMSO. Stock solutions were stored at −20 °C.

Cell Culture. A549 (CCL-185; gender: male) and HT-1080 (CCL-121; gender: male) cells were obtained from ATCC, expanded for one passage, and then frozen down in multiple aliquots used for all subsequent experiments. Mouse embryonic fibroblasts (gender: not specified), derived from wild-type and KO animals and immortalized using SV40, were a kind gift from Tadashi Suzuki, RIKEN, Saitama, Japan. Paired unmodified control and NGLY1^{KO} HEK293 and HepG2 cells were a kind gift from Grace Science, LLC. A549 CRISPR-Cas9 Control1/2 cells and NFE2L1$^{KO1/2}$, NGLY1$^{LOF1/2}$, NFE2L2$^{KO1/2}$, and HT-1080 GPX4$^{KO1/2}$ cells expressing nuclear-localized mKate2 were generated as described below. Polyclonal populations of these cell lines were generated from the respective parental cells via transduction with the NucLight Red lentivirus, which directs the expression of nuclear-localized mKate2 (Essen BioScience/Sartorius). Cell lines expressing nuclear-localized mKate2 are distinguished from the parental cell lines by a superscripted N notation, which sometimes may also be combined with an indication of the gene disruption. For example, NFE2L1^{KO1,N} would refer to the first clonal NFE2L1 gene-disrupted cell line, which was engineered to express nuclear-localized mKate2. Polyclonal mKate2-expressing cells were selected for using fluorescence-activated cell sorting (FACS) (Stanford Shared FACS Facility). All cells were grown in Dulbecco's modified Eagle's medium (DMEM; MT-10-013-CV; Thermo Fisher Scientific) supplemented with 10% fetal bovine serum (FBS; 26140-079; Gibco) and 0.5 U/mL penicillin/streptomycin (P/S; 15070-063; Gibco). HT-1080 cells were additionally supplemented with 1% MEM nonessential amino acids (11140-050; Life Technologies). Phosphate-buffered saline (PBS; 1×; 97062-338) was from VWR, and trypsin (25200114) was from Gibco. For all experiments, cells were trypsinized and counted using a Cellometer Auto T4 cell counter (Nexcelom).

Genotype Drug Sensitivity Analysis. Data for cell line *KEAP1* mutation status and sensitivity to erastin and RSL3 (from the CTD^2 program) were downloaded from the DepMap portal (https://depmap.org/portal/; 19 July 2021).

Generation of Clonal CRISPR-Cas9 Gene-Disrupted Cells. The following single-guide RNA (sgRNA) primer sets were used to generate clonal *NFE2L1*, *NGLY1*, *NFE2L2*, and *GPX4* gene-disrupted cell lines, which we refer to as either KO or LOF: *NFE2L1* (exon 2): forward, 5′-CACCgTTTCTCGCACCCCGTTGTCT-3′ and reverse, 5′-AAACAGACAACGGGGTGCGAGAAAc-3′; *NGLY1* (exon 2): forward, 5′-CACCgAAATATAGATCCATCCGGAT-3′ and reverse, 5′-AAACATCCGGATGGATCTATATTTc-3′; *NFE2L2* (exon 2): forward, 5′-CACCgATTTGATTGACATACTTTGG-3′ and reverse, 5′-AAACCCAAAGTATGTCAATCAAATc-3′; and *GPX4* (exon 3): forward, 5′-CACGCCCGATACGCTGAGTG-3′ and reverse, 5′-CACTCAGCGTATCGGGCGTGc-3′. sgRNAs were cloned into pSpCas9(BB)-2A-GFP, a kind gift from Jan Carette, Stanford University School of Medicine, as described (51). Briefly, primers were annealed by heating to 95 °C, then cooled by 2.5 °C/min to 25 °C. The resulting oligo duplex was diluted 1:200 in ddH_2O and used for cloning into the pSpCas9(BB) plasmid. The ligation reaction contained the following: 100 ng pSpCas9(BB), 2 μL of the diluted oligo duplex, 2 μL 10× FastDigest buffer (Thermo Fisher Scientific), 1 μL 10 mM dithiothreitol, 1 μL 10 mM adenosine triphosphate, 1 μL FastDigest *Bpi*I (D1014; Thermo Fisher Scientific), 0.5 μL T4 DNA ligase (EL0014; Thermo Fisher Scientific), and 12.5 μL ddH_2O to produce a final reaction volume of 20 μL. The ligation reaction was incubated for 1 h ([37 °C, 5 min; 21 °C, 5 min] × six cycles). Two microliters of the product was used to transform competent DH5α cells on LB-amp (100 μg/mL) plates. Plasmid DNA was extracted using a spin column (27106; Qiagen) and confirmed via Sanger sequencing. Cells were transfected with 2.5 μg DNA using Opti-MEM I Reduced Serum Medium (31985-062; Life Technologies) and Lipofectamine LTX Reagent with PLUS Reagent (15338-100; Life Technologies), according to the manufacturer's instructions. The next day the medium was replaced, and the cells were allowed to recover for 24 h. Transfected cells were then trypsinized, washed in 1× PBS, and sorted for green fluorescent protein–positive (GFP$^+$) cells with a Carmen cell sorter (BD Biosciences) (Stanford Shared FACS Facility) into a 96-well plate prefilled with DMEM containing 30% FBS and 0.5 U/mL P/S. Cells were incubated at 37 °C until distinct clones appeared. Individual clones were amplified in normal (10% FBS) medium to produce enough cells for protein analysis. Clones were validated by Western blot to confirm loss of protein expression. HT-1080 GPX4$^{KO1/2}$ clones were cultured in medium supplemented with 1 μM Fer-1 to inhibit ferroptosis.

Generation of Stable Overexpression Cell Lines. The cDNA of human NGLY1 was subcloned from a pLex-NGLY1 construct, described previously (26), into the lentiviral expression plasmid pLenti-CMV-Puro DEST (Addgene plasmid 17452; from Eric Campeau and Paul Kaufman, University of Massachusetts Medical School, Worcester, MA) via Gibson assembly using a commercial kit (E2611S; New England Biolabs). Lentiviral constructs for NFE2L1 and protein sequence–edited NFE2L1^{8ND} were synthesized (Twist Biosciences). The open reading frame (ORF) for NFE2L2 was obtained from Aaron Gitler (Stanford School of Medicine, Stanford, CA) as a pDONR plasmid from the human ORFeome library. The NFE2L2 ORF was cloned into the pLenti-CMV-Puro vector using a Gateway LR Clonase II Kit (11791-020; Thermo Fisher Scientific). The cGPX4 construct pLenti-CMV-Hygro-cGPX4 was the kind gift of Brent Stockwell, Columbia University, New York, NY, and James Olzmann, University of California, Berkeley, CA. pLenti-CMV-Puro was used as an EV control for comparison in overexpression experiments. All plasmids were verified by Sanger sequencing. Lentiviruses were generated in HEK293T cells using a third-generation lentivirus packaging system. Briefly, cells were transfected with 1 μg pLenti-CMV DEST plasmid + 0.25 mg of each of three third-generation lentiviral packaging plasmids (pMDLg/pRRE, pRSV-Rev, and pMD2.G; Addgene plasmids 12251, 12253, and 12259, respectively; from Didier Trono, École Polytechnique Fédérale de Lausanne, Lausanne, Switzerland) using PolyJet DNA Transfection Reagent (SignaGen Laboratories; SL100688) per the manufacturer's instructions. Lentivirus was harvested twice (3 and 4 d posttransfection), filtered through a 0.45-μm polyvinylidene fluoride filter (SLHV033RS; Merck Millipore), and stored at −80 °C until use. For infections, 0.5 mL of freshly thawed virus soup was mixed with Polybrene (H9268; Sigma-Aldrich) to a final concentration of 8 μg/mL and used to infect A549^{N} and HT-1080^{N} cell lines. Stably transduced cell populations were selected with 1.25 μg/mL puromycin (A11138-03; Life Technologies) for 2 d.

NGLY1^{L408X} Mutagenesis. The NGLY1^{L408X} mutant was generated using the Q5 Site-Directed Mutagenesis Kit (E0552S; New England Biolabs) using the pLenti-CMV-Puro-NGLY1 construct, described above, with the following primers following the manufacturer's instructions: forward, 5′-GGTGATTGCCTGAAGAACTAAGG-3′ and reverse, 5′-TCTTCATGTTTGCAGGAATATC-3′. The resultant pLenti-CMV-Puro-NGLY1^{L408X} construct was verified by Sanger sequencing. Lentivirus harboring this construct was generated as described above.

Western Blotting. Three hundred thousand cells per well were seeded into duplicate wells of 6-well plates (Thermo Fisher Scientific; 07-200-83) in 2 mL medium. For Western blots with bortezomib induction, the day after seeding, media were replaced with 2 mL media containing either DMSO or bortezomib (200 nM final). For Western blots probing NFE2L1 induction with ferroptosis-inducing compounds, media were replaced with fresh media containing DMSO, erastin2 (4 μM), ML162 (4 μM), bortezomib (200 nM), erastin2 and bortezomib, or ML162 and bortezomib. After 4 h, cells were washed once with 1× PBS (VWR; 97062-338), harvested by cell scraping using 300 μL trypsin per well (Gibco; 25200114), and quenched with 600 μL complete medium. Duplicate wells were combined in a 2-mL collection tube (Thermo Fisher Scientific; 05-408-138) and pelleted by spinning cells at 500 × *g* for 5 min. Pellets were washed with 1 mL of 1× PBS and lysed with 100 μL of 9 M urea (U5378; Sigma-Aldrich). Lysates were subsequently sonicated and spun for 15 min in a centrifuge at maximum speed. Supernatants were collected and transferred to a fresh 1.5-mL Eppendorf tube, and protein abundance was quantified with the bicinchoninic acid assay. Thirty micrograms of protein from each lysate was loaded onto a Bolt 4 to 12% Bis-Tris Plus sodium dodecyl sulfate gel (Life Technologies) for separation for 75 min at 100 V. The gel was transferred to a nitrocellulose membrane using the iBlot2 System (Life Technologies). Membranes were probed with primary antibody overnight in a hybridization bag at 4 °C. Antibody dilutions (and suppliers) were as follows: alpha-tubulin DM1A (1:5,000; Thermo Fisher Scientific; MS581P1), TCF11/NRF1/NFE2L1 D5B10 (1:1,000; Cell Signaling Technology; 8052S), NGLY1 (1:500; Sigma-Aldrich; HPA036825), NRF2/NFE2L2 (1:1,000; Abcam; ab137550), H5 γ-GCSc/GCLC (1:1,000; Santa Cruz Biotechnology; 390811), GCLM (1:1,000; GeneTex; GTX114075), HO-1 EPR18161-128 (1:1,000; Abcam; ab189491), CPS1 EPR7493-3 (1:1,000; Abcam; ab129076), and GPX4 EPNCIR144 (1:1,000; Abcam; ab125066). Donkey anti-rabbit secondary antibody (IRDye 800LT; LI-COR Biosciences) and donkey anti-mouse antibody (IRDye 680LT; LI-COR Biosciences) were used at 1:15,000 dilution to visualize bands. Membranes were imaged using the LI-COR CLx Imaging System.

Western Blot Quantification. After membranes were imaged using the LI-COR CLx Imaging System, densitometry was performed using Image Studio Lite (version 5.2.5) using the analysis tool. Briefly, the signals of tubulin and proteins of interest were extracted from each channel. Proteins of interest were normalized to tubulin signal. In experiments that used two independent control lines, protein levels were normalized to the average observed for both control lines. Quantifications are reported from multiple independent experiments conducted on different days.

Cell Death Experiments. The day prior to the start of an experiment, 1,500 cells per well were seeded into a 384-well plate (Corning; 3764) in 45 μL media. The next day, the media were removed and replaced with 45 μL medium containing SYTOX Green (20 nM final) and 5 μL of 10× compound prepared in a 384-well storage plate (Thermo Fisher Scientific; AB-0781). Experiments with paired HEK293 and HepG2 control and NGLY1 KO cells were performed by seeding 7,500 cells per well into a 96-well plate (Thermo Fisher Scientific; 07-200-588) in 200 μL medium; 96-well plate experiments with A549 or HT-1080 cells were seeded at a density of 4,000 cells per well. For 96-well plate experiments, the day after seeding, 20 μL of 10× compound was added to 180 μL of fresh media containing SYTOX Green (20 nM final). The next day the medium was removed and replaced with 180 μL medium containing SYTOX Green (20 nM final) and 20 μL of 10× compound.

Analysis of Cell Death. In several small-scale experiments, we examined cell death using an adapted STACK approach, as described previously (41), using an IncuCyte Zoom dual-color live content imaging system (4459; Essen BioScience/Sartorius) housed within a Thermo tissue-culture incubator (37 °C, 5% CO_2). The STACK approach uses an automated microscope to measure cell death over time in populations of cells. Cells of interest are engineered to express nuclear-localized mKate2 protein, which is used as a proxy for live cells. Cells are treated in medium containing the dead-cell dye SYTOX Green (20 nM final), which is normally excluded from live cells but upon membrane permeabilization will enter the nucleus, intercalate with DNA, and undergo a conformational change that enhances fluorescence emission. Lethal fraction, a measure of population cell death, is computed by taking 1 minus the fraction of dead cells (SYTOX Green–positive) over total cells in the population (SYTOX Green–positive + mKate2-positive). Some cells transiently are both mKate2- and SYTOX Green–positive and these overlapping counts are subtracted from mKate2-positive object counts (41, 52). Images were acquired using a 10× objective lens in phase contrast, green fluorescence (excitation [ex]: 460 ± 20; emission [em]: 524 ± 20; acquisition time: 400 ms), and red fluorescence (ex: 585 ± 20; em: 665 ± 40; acquisition time: 800 ms) channels. For each well, images (1,392 × 1,040 pixels at 1.22 μm per pixel) were acquired every 2 or 4 h for a variable length of time, depending on the experiment. Automated object detection was performed in parallel to data acquisition using the Zoom software package (V2016A/B) using a routine with the following settings (in parentheses) to count mKate2-positive objects (parameter adaptive, threshold adjustment 1; edge split on; edge sensitivity 80; filter area minimum 100 μm^2; mean intensity minimum 3.0), SYTOX Green–positive objects (parameter adaptive, threshold adjustment 1; edge split on; edge sensitivity −5; filter area minimum 20 μm^2, maximum 750 μm^2; eccentricity maximum 1.0; mean intensity minimum 1.0), and overlap (e.g., mKate2-positive and SYTOX Green–positive) objects (filter area minimum 20 μm^2, maximum 5,000 μm^2). Some experiments employed unmarked cells and SYTOX Green–positive cells only were counted as a metric of cell death.

Small Molecule Library Screen. The day before compound addition, 1,500 A549 Control1^{N}, NFE2L1^{KO1,N}, and NFE2L1^{KO2,N} cells per well were seeded into three 384-well plates in 45 μL medium. The next day, the medium was removed and replaced with medium containing SYTOX Green (20 nM final), and compounds from a freshly thawed library master stock plate (one compound per well) were added to a final concentration of 5 μM. Plates were imaged immediately and every 4 h thereafter for a total of 96 h using Essen IncuCyte Zoom. Counts of SYTOX Green and mKate2 objects per square millimeter were obtained and the lethal fraction was calculated as described above. The AUC values of

lethal fraction scores across the full 96 h were calculated using the trapezoid rule in Microsoft Excel (version 16.44). AUC values were normalized to yield normalized AUC (nAUC) values as described (42). Briefly, nAUC = observed AUC/theoretical AUC. The theoretical AUC is equivalent to the number of hours for a given treatment, in this case 96 h. Thus, the theoretical AUC = 96 (e.g., lethal fraction = 1 at time = 0 h for an experiment that lasts 96 h = 96 AUC units).

RNA-Seq. A549 Control1^{N}, NFE2L1^{KO1,N}, and NFE2L1^{KO2,N} cells were seeded into 6-well dishes at 200,000 cells per well. Cells were treated with either DMSO or bortezomib (200 nM) for 4 h. Cells were subsequently washed with ice-cold 1× PBS and harvested on ice by cell scraping. The cell solution was pelleted at 500 × *g* for 5 min. Following centrifugation, the supernatant was removed, and cells were lysed for RNA extraction using a Qiashredder column (79654; Qiagen) and RNeasy Plus RNA Extraction Kit (74134; Qiagen). Two biological replicates were collected per genotype and treatment condition. Purity, concentration, and integrity of RNA were assessed by a NanoDrop spectrophotometer (Thermo Fisher Scientific) and by Eukaryote Total RNA Nano chip analysis using a Bioanalyzer (Agilent) at the Stanford Protein and Nucleic Acid Facility. The RNA integrity number for each sample met or exceeded the minimum threshold of 6.8. Samples were then shipped on dry ice to Novogene for library generation and 20M read PE150 sequencing on an Illumina HiSeq 4000 platform. Data cleanup was performed by excluding reads with adaptor contamination, >10% of indeterminate bases, or >50% bases with a quality score ≤5. The remaining reads (≥98% of all reads across all conditions) were aligned to the hg19 human reference genome using STAR. At least 91% of clean reads were mapped across all conditions. Pearson correlation between biological replicates was $R^2 \geq 0.96$ for all samples. Differential gene expression was calculated using DESeq 1.10.1. We selected all protein-coding genes with read counts above 0.5 fragments per kilobase million in all conditions and with significant alterations (adjusted *P* value < 0.05). All RNA-seq data were deposited in the GEO with accession number GSE182461.

qRT-PCR. Three hundred thousand cells were seeded into a 6-well plate. The next day, cells were washed twice with ice-cold 1× PBS and scraped to harvest. RNA was extracted using a Qiashredder extraction column (Qiagen; 79654) and the RNeasy Plus RNA Extraction Kit (74134; Qiagen). cDNA was generated using the TaqMan Reverse Transcriptase Kit according to the manufacturer's instructions (N8080234; Thermo Fisher Scientific). qPCR reactions were prepared with SYBR Green Master Mix (4367659; Life Technologies) and run on an Applied Biosystems QuantStudio 3 real-time PCR machine (Thermo Fisher Scientific). Relative transcript levels were calculated using the ΔΔCT method and normalized to the *ACTB* gene. The following primers were used to amplify *ACTB*: forward, 5′-CATGTACGTTGCTATCCAGGC-3′ and reverse, 5′-CTCCTTAATGTCACGCACGAT-3′; the following primers were used to amplify *GPX4*: forward, 5′-AGACCGAAGTAAACTACACTCAGC-3′ and reverse, 5′-CGGCGAACTCTTTGATCTCT-3′.

GSH Measurement by Liquid Chromatography Coupled to Mass Spectrometry. Cells were washed with 1.5 mL per well of 0.9% saline solution in water (over ice) and then harvested with 1 mL per well of 80% methanol (on dry ice) with 500 nM ^{13}C- and ^{15}N-labeled amino acids (MSK-A1-1.2; Cambridge Isotope Laboratories) as internal standards. Whole-cell harvest was then transferred to prechilled microcentrifuge tubes and stored at −80 °C. On the day of analysis, samples were vortexed for 10 min at 4 °C. Clear supernatant was then transferred to polypropylene autosampler vials after centrifugation for 10 min at 15,000 rpm at 4 °C. Polar metabolite profiling was performed on an ID-X Tribrid mass spectrometer (Thermo Fisher Scientific) with an electrospray ionization probe. Hydrophilic interaction chromatography (HILIC) on a SeQuant ZIC-pHILIC 150 × 2.1-mm column (Millipore Sigma; 1504600001) coupled with a 20 × 2.1-mm guard (Millipore Sigma; 1504380001) was used to separate polar metabolites prior to mass spectrometry analysis. Mobile phase A consisted of 20 mM ammonium carbonate and 0.1% ammonium hydroxide in water, and mobile phase B was pure acetonitrile. HILIC was performed at a flow rate of 0.15 mL/min with the following gradient: linear decrease from 80 to 20% B from 0 to 20 min, linear increase from 20 to 80% B from 20 to 20.5 min, hold at 80% B from 20.5 to 28 min. A full scan from *m/z* 70 to 1,000 with polarity switching was used for the mass spectrometer. Ion transfer tube and vaporizer temperatures were set to 275 and 350 °C, respectively. An Orbitrap resolution at 120,000, radio frequency lens at 40%, automatic gain control target at 1×10^6, and maximum injection time of 80 ms were used. Positive- and negative-ion voltages were 3,000 and 2,500 V, respectively. Sheath gas at 40 units, aux gas at 15 units, and sweep gas at 1 unit were set for the ion source. EASY-ICTM was enabled for internal mass calibration. Metabolite abundance was quantified by TracerFinder (Thermo Fisher Scientific) using an in-house library of known metabolite standards. A mass tolerance of 5 parts per million was used for extracting ion chromatograms.

HT-1080 Control^{N} and GPX4^{KO} Fer-1 Withdrawal Experiments. Eight thousand HT-1080^{N} cells expressing an EV, NFE2L1, or NFE2L2 were seeded into four replicate wells per genotype in a 96-well plate (Thermo Fisher Scientific; 07-200-588). The seeding density of each well was 8,000 cells per well in 200 μL of media containing 1 μM Fer-1. The next day, the medium was removed, and cells were washed three times with 200 μL of 1× PBS. After the third wash, two wells per genotype received medium containing SYTOX Green (20 nM final) ± Fer-1 (1 μM). Cell death was then determined using STACK over 48 h.

Statistics. Where applicable, unpaired *t* tests were performed using GraphPad Prism (version 9.1.0). *$P \leq 0.05$, **$P \leq 0.01$, ***$P \leq 0.001$.

Data Availability. The RNA-seq data reported in this article have been deposited in the GEO (accession no. GSE182461).

All study data are included in the article and/or *SI Appendix*.

ACKNOWLEDGMENTS. We thank J. Carette, A. Gitler, B. Stockwell, and J. Olzmann for sharing reagents. G.C.F. was supported by the Stanford ChEM-H Chemistry/Biology Interface Predoctoral Training Program. This work was also supported by the Grace Science Foundation (C.R.B. and S.J.D.), a Stanford Cancer Institute Award (to M.A.-R.), and the NIH (R01CA227942 and U01 CA226051-01A1 to C.R.B.; R01GM122923 to S.J.D.).

Author affiliations: [a]Department of Biology, Stanford University, Stanford, CA 94305; [b]Department of Chemical Engineering, Stanford University, Stanford, CA 94305; [c]Stanford ChEM-H, Stanford University, Stanford, CA 94305; [d]Department of Chemistry, Stanford University, Stanford, CA 94305; and [e]HHMI, Stanford University, Stanford, CA 94305

1. X. Jiang, B. R. Stockwell, M. Conrad, Ferroptosis: Mechanisms, biology and role in disease. *Nat. Rev. Mol. Cell Biol.* **22**, 266–282 (2021).
2. W. S. Yang *et al.*, Regulation of ferroptotic cancer cell death by GPX4. *Cell* **156**, 317–331 (2014).
3. J. I. Leu, M. E. Murphy, D. L. George, Mechanistic basis for impaired ferroptosis in cells expressing the African-centric S47 variant of p53. *Proc. Natl. Acad. Sci. U.S.A.* **116**, 8390–8396 (2019).
4. M. A. Badgley *et al.*, Cysteine depletion induces pancreatic tumor ferroptosis in mice. *Science* **368**, 85–89 (2020).
5. S. J. Dixon *et al.*, Ferroptosis: An iron-dependent form of nonapoptotic cell death. *Cell* **149**, 1060–1072 (2012).
6. L. Magtanong *et al.*, Exogenous monounsaturated fatty acids promote a ferroptosis-resistant cell state. *Cell Chem. Biol.* **26**, 420–432.e9 (2019).
7. G. P. Sykiotis, D. Bohmann, Stress-activated cap'n'collar transcription factors in aging and human disease. *Sci. Signal.* **3**, re3 (2010).
8. N. Liu, X. Lin, C. Huang, Activation of the reverse transsulfuration pathway through NRF2/CBS confers erastin-induced ferroptosis resistance. *Br. J. Cancer* **122**, 279–292 (2020).
9. N. Takahashi *et al.*, 3D culture models with CRISPR screens reveal hyperactive NRF2 as a prerequisite for spheroid formation via regulation of proliferation and ferroptosis. *Mol. Cell* **80**, 828–844.e6 (2020).
10. M. Dodson, R. Castro-Portuguez, D. D. Zhang, NRF2 plays a critical role in mitigating lipid peroxidation and ferroptosis. *Redox Biol.* **23**, 101107 (2019).
11. F. Kuang, J. Liu, Y. Xie, D. Tang, R. Kang, MGST1 is a redox-sensitive repressor of ferroptosis in pancreatic cancer cells. *Cell Chem. Biol.* **28**, 765–775.e5 (2021).
12. Z. Fan *et al.*, Nrf2-Keap1 pathway promotes cell proliferation and diminishes ferroptosis. *Oncogenesis* **6**, e371 (2017).
13. X. Sun *et al.*, Activation of the p62-Keap1-NRF2 pathway protects against ferroptosis in hepatocellular carcinoma cells. *Hepatology* **63**, 173–184 (2016).
14. Y. P. Kang *et al.*, Non-canonical glutamate-cysteine ligase activity protects against ferroptosis. *Cell Metab.* **33**, 174–189.e7 (2021).
15. S. Vomund, A. Schäfer, M. J. Parnham, B. Brüne, A. von Knethen, Nrf2, the master regulator of anti-oxidative responses. *Int. J. Mol. Sci.* **18**, 2772 (2017).
16. K. Chan, R. Lu, J. C. Chang, Y. W. Kan, NRF2, a member of the NFE2 family of transcription factors, is not essential for murine erythropoiesis, growth, and development. *Proc. Natl. Acad. Sci. U.S.A.* **93**, 13943–13948 (1996).
17. J. Y. Chan *et al.*, Targeted disruption of the ubiquitous CNC-bZIP transcription factor, Nrf-1, results in anemia and embryonic lethality in mice. *EMBO J.* **17**, 1779–1787 (1998).
18. M. Kwong, Y. W. Kan, J. Y. Chan, The CNC basic leucine zipper factor, Nrf1, is essential for cell survival in response to oxidative stress-inducing agents. Role for Nrf1 in gamma-gcs(l) and gss expression in mouse fibroblasts. *J. Biol. Chem.* **274**, 37491–37498 (1999).

19. L. Chen *et al.*, Nrf1 is critical for redox balance and survival of liver cells during development. *Mol. Cell. Biol.* **23**, 4673–4686 (2003).
20. L. Leung, M. Kwong, S. Hou, C. Lee, J. Y. Chan, Deficiency of the Nrf1 and Nrf2 transcription factors results in early embryonic lethality and severe oxidative stress. *J. Biol. Chem.* **278**, 48021–48029 (2003).
21. J. Steffen, M. Seeger, A. Koch, E. Krüger, Proteasomal degradation is transcriptionally controlled by TCF11 via an ERAD-dependent feedback loop. *Mol. Cell* **40**, 147–158 (2010).
22. S. K. Radhakrishnan *et al.*, Transcription factor Nrf1 mediates the proteasome recovery pathway after proteasome inhibition in mammalian cells. *Mol. Cell* **38**, 17–28 (2010).
23. K. Itoh *et al.*, Keap1 represses nuclear activation of antioxidant responsive elements by Nrf2 through binding to the amino-terminal Neh2 domain. *Genes Dev.* **13**, 76–86 (1999).
24. S. B. Cullinan, J. D. Gordan, J. Jin, J. W. Harper, J. A. Diehl, The Keap1-BTB protein is an adaptor that bridges Nrf2 to a Cul3-based E3 ligase: Oxidative stress sensing by a Cul3-Keap1 ligase. *Mol. Cell. Biol.* **24**, 8477–8486 (2004).
25. A. L. Eggler, E. Small, M. Hannink, A. D. Mesecar, Cul3-mediated Nrf2 ubiquitination and antioxidant response element (ARE) activation are dependent on the partial molar volume at position 151 of Keap1. *Biochem. J.* **422**, 171–180 (2009).
26. F. M. Tomlin *et al.*, Inhibition of NGLY1 inactivates the transcription factor Nrf1 and potentiates proteasome inhibitor cytotoxicity. *ACS Cent. Sci.* **3**, 1143–1155 (2017).
27. A. B. Dirac-Svejstrup *et al.*, DDI2 is a ubiquitin-directed endoprotease responsible for cleavage of transcription factor NRF1. *Mol. Cell* **79**, 332–341.e7 (2020).
28. N. J. Lehrbach, P. C. Breen, G. Ruvkun, Protein sequence editing of SKN-1A/Nrf1 by peptide:N-glycanase controls proteasome gene expression. *Cell* **177**, 737–750.e15 (2019).
29. P. Lipari Pinto *et al.*, NGLY1 deficiency–A rare congenital disorder of deglycosylation. *JIMD Rep.* **53**, 2–9 (2020).
30. J. Kong *et al.*, Mitochondrial function requires NGLY1. *Mitochondrion* **38**, 6–16 (2018).
31. K. Yang, R. Huang, H. Fujihira, T. Suzuki, N. Yan, N-glycanase NGLY1 regulates mitochondrial homeostasis and inflammation through NRF1. *J. Exp. Med.* **215**, 2600–2616 (2018).
32. S. Y. Han *et al.*, A conserved role for AMP-activated protein kinase in NGLY1 deficiency. *PLoS Genet.* **16**, e1009258 (2020).
33. D. M. Talsness *et al.*, A *Drosophila* screen identifies NKCC1 as a modifier of NGLY1 deficiency. *eLife* **9**, e57831 (2020).
34. M. A. Tambe, B. G. Ng, H. H. Freeze, N-glycanase 1 transcriptionally regulates aquaporins independent of its enzymatic activity. *Cell Rep.* **29**, 4620–4631.e4 (2019).
35. A. Galeone *et al.*, Regulation of BMP4/Dpp retrotranslocation and signaling by deglycosylation. *eLife* **9**, e55596 (2020).
36. K. G. Owings, J. B. Lowry, Y. Bi, M. Might, C. Y. Chow, Transcriptome and functional analysis in a *Drosophila* model of NGLY1 deficiency provides insight into therapeutic approaches. *Hum. Mol. Genet.* **27**, 1055–1066 (2018).
37. A. Tsherniak *et al.*, Defining a cancer dependency map. *Cell* **170**, 564–576.e16 (2017).
38. F. M. Behan *et al.*, Prioritization of cancer therapeutic targets using CRISPR-Cas9 screens. *Nature* **568**, 511–516 (2019).
39. J. Y. Cao *et al.*, A genome-wide haploid genetic screen identifies regulators of glutathione abundance and ferroptosis sensitivity. *Cell Rep.* **26**, 1544–1556.e8 (2019).
40. H. Dreger *et al.*, Nrf2-dependent upregulation of antioxidative enzymes: A novel pathway for proteasome inhibitor-mediated cardioprotection. *Cardiovasc. Res.* **83**, 354–361 (2009).
41. G. C. Forcina, M. Conlon, A. Wells, J. Y. Cao, S. J. Dixon, Systematic quantification of population cell death kinetics in mammalian cells. *Cell Syst.* **4**, 600–610.e6 (2017).
42. M. Conlon *et al.*, A compendium of kinetic modulatory profiles identifies ferroptosis regulators. *Nat. Chem. Biol.* **17**, 665–674 (2021).
43. Y. Yoshida *et al.*, Loss of peptide:N-glycanase causes proteasome dysfunction mediated by a sugar-recognizing ubiquitin ligase. *Proc. Natl. Acad. Sci. U.S.A.* **118**, e2102902118 (2021).
44. S. C. Lu, Glutathione synthesis. *Biochim. Biophys. Acta* **1830**, 3143–3153 (2013).
45. J. I. Leu, M. E. Murphy, D. L. George, Functional interplay among thiol-based redox signaling, metabolism, and ferroptosis unveiled by a genetic variant of *TP53*. *Proc. Natl. Acad. Sci. U.S.A.* **117**, 26804–26811 (2020).
46. A. Tarangelo *et al.*, p53 suppresses metabolic stress-induced ferroptosis in cancer cells. *Cell Rep.* **22**, 569–575 (2018).
47. L. Jiang *et al.*, Ferroptosis as a p53-mediated activity during tumour suppression. *Nature* **520**, 57–62 (2015).
48. W. H. Yang *et al.*, The Hippo pathway effector TAZ regulates ferroptosis in renal cell carcinoma. *Cell Rep.* **28**, 2501–2508.e4 (2019).
49. J. Wu *et al.*, Intercellular interaction dictates cancer cell ferroptosis via NF2-YAP signalling. *Nature* **572**, 402–406 (2019).
50. S. Iyer *et al.*, Drug screens of *NGLY1* deficiency in worm and fly models reveal catecholamine, NRF2 and anti-inflammatory-pathway activation as potential clinical approaches. *Dis. Model. Mech.* **12**, dmm040576 (2019).
51. F. A. Ran *et al.*, Genome engineering using the CRISPR-Cas9 system. *Nat. Protoc.* **8**, 2281–2308 (2013).
52. Z. Inde, J. Rodencal, S. J. Dixon, Quantification of drug-induced fractional killing using high-throughput microscopy. *STAR Protoc.* **2**, 100300 (2021).